

Surface Wave Dispersion Measurements and Tomography from Ambient Seismic Noise Correlation in China

Xiaodong Song

**University of Illinois at Urbana-Champaign
1901 S. Research Park, Suite A
Champaign, IL 61820**

Final Report

15 March 2010

APPROVED FOR PUBLIC RELEASE; DISTRIBUTION IS UNLIMITED.



**AIR FORCE RESEARCH LABORATORY
Space Vehicles Directorate
29 Randolph Rd
AIR FORCE MATERIEL COMMAND
HANSCOM AFB, MA 01731-3010**

NOTICES

Using Government drawings, specifications, or other data included in this document for any purpose other than Government procurement does not in any way obligate the U.S. Government. The fact that the Government formulated or supplied the drawings, specifications, or other data does not license the holder or any other person or corporation; or convey any rights or permission to manufacture, use, or sell any patented invention that may relate to them.

This report was cleared for public release and is available to the general public, including foreign nationals. Qualified requestors may obtain copies of this report from the Defense Technical Information Center (DTIC) (<http://www.dtic.mil>). All others should apply to the National Technical Information Service.

AFRL-RV-HA-TR-2010-1023 HAS BEEN REVIEWED AND IS APPROVED FOR PUBLICATION IN ACCORDANCE WITH ASSIGNED DISTRIBUTION STATEMENT.

//signature//

ROBERT J. RAISTRICK
Contract Manager

//signature//

Domenic Thompson, Maj, USAF, Chief
Battlespace Surveillance Innovation Center

This report is published in the interest of scientific and technical information exchange, and its publication does not constitute the Government's approval or disapproval of its ideas or findings.

REPORT DOCUMENTATION PAGE				Form Approved OMB No. 0704-0188	
Public reporting burden for this collection of information is estimated to average 1 hour per response, including the time for reviewing instructions, searching existing data sources, gathering and maintaining the data needed, and completing and reviewing this collection of information. Send comments regarding this burden estimate or any other aspect of this collection of information, including suggestions for reducing this burden to Department of Defense, Washington Headquarters Services, Directorate for Information Operations and Reports (0704-0188), 1215 Jefferson Davis Highway, Suite 1204, Arlington, VA 22202-4302. Respondents should be aware that notwithstanding any other provision of law, no person shall be subject to any penalty for failing to comply with a collection of information if it does not display a currently valid OMB control number. PLEASE DO NOT RETURN YOUR FORM TO THE ABOVE ADDRESS.					
1. REPORT DATE (DD-MM-YYYY) 15-03-2010		2. REPORT TYPE Final Report		3. DATES COVERED (From - To) 20-12-2007 to 31-20-2009	
4. TITLE AND SUBTITLE Surface Wave Dispersion Measurements and Tomography from Ambient Seismic Noise in China				5a. CONTRACT NUMBER FA8718-07-C-0006	
				5b. GRANT NUMBER	
				5c. PROGRAM ELEMENT NUMBER 62601F	
6. AUTHOR(S) Xiaodong Song				5d. PROJECT NUMBER 1010	
				5e. TASK NUMBER SM	
				5f. WORK UNIT NUMBER A1	
7. PERFORMING ORGANIZATION NAME(S) AND ADDRESS(ES) Dept. of Geology, U. of Illinois at Urbana-Champaign 1301 W. Green St. 253 NHB Urbana, IL 61801				8. PERFORMING ORGANIZATION REPORT NUMBER	
9. SPONSORING / MONITORING AGENCY NAME(S) AND ADDRESS(ES) Air Force Research Laboratory 29 Randolph Rd. Hanscom AFB, MA 01731-3010				10. SPONSOR/MONITOR'S ACRONYM(S) AFRL/RVBYE	
				11. SPONSOR/MONITOR'S REPORT NUMBER(S) AFRL-RV-HA-TR-2010-1023	
12. DISTRIBUTION / AVAILABILITY STATEMENT Approved for Public Release; Distribution Unlimited.					
13. SUPPLEMENTARY NOTES					
14. ABSTRACT We performed ambient noise tomography of China using the data from the China National Seismic Network and surrounding global and PASSCAL-type stations. For most of the station pairs, we retrieve good Rayleigh waveforms from ambient noise correlations using a few months to several years of continuous data at all distance ranges across the entire region (over 5000 km) and for periods from about 70 s down to about 8 s. We obtained a total number of 33,800 station-pairs (paths) and measured Rayleigh wave group and phase velocities. We inverted the Rayleigh wave dispersion measurements for dispersion maps at periods from 8 to 70 s. The dispersion maps correlate nicely with surface geology. A major feature of the ambient noise method is that the whole process is completely repeatable with different time segments, which make it possible to evaluate the uncertainties. We adopt a bootstrap method to quantify the errors in the Rayleigh wave group velocity dispersion measurements and the tomographic maps. Most of the pairs show similar dispersion curves between different runs and small standard deviations, indicating good data quality and convergence of the Green function. Group velocity at long period end generally has a larger error, which is consistent with the notion that the long period needs longer time to converge. The best retrieved periods are from 10 to 30 s with the optimal period of around 15 to 20 s. We invert the Rayleigh group and phase dispersion maps for 3D shear-wave velocity structure. The 3D model shows some remarkable features that correlate with surface geology.					
15. SUBJECT TERMS Ambient noise tomography, Rayleigh wave dispersion, China Seismic Network					
16. SECURITY CLASSIFICATION OF:			17. LIMITATION OF ABSTRACT	18. NUMBER OF PAGES	19a. NAME OF RESPONSIBLE PERSON
a. REPORT UNC	b. ABSTRACT UNC	c. THIS PAGE UNC			Robert Raistrick
			SAR	22	19b. TELEPHONE NUMBER (include area code) 781-377-3726

Table of Contents

1. Summary	1
2. Introduction	1
3. Technical Approach	2
3.1. Ambient noise tomography method	2
3.2. Data	4
4. Results and Discussion	4
4.1. Dispersion measurements	4
4.2. Rayleigh wave tomography	6
4.3. 3D shear-wave structure	7
4.4. Validation and error analyses	9
5. Conclusions	13
References	15
List of Symbols, Abbreviations, and Acronyms	16

List of Figures

1. Map of seismic stations used in this study	3
2. Example of EGF and dispersion measurement from ambient noise	5
3. Dispersion measurement histogram and ray density map	5
4. Maps of Rayleigh wave group velocities obtained in this study	6
5. Resolution maps of Rayleigh wave group velocities	7
6. S wave model from inversion of dispersion maps	8
7. S velocities of our model at the depth of CRUST 2.0 Moho	9
8. Crustal thickness map obtained in this study	9
9. Temporal and spatial consistency of dispersion measurements	11
10. Example of model validation	12
11. Examples of error estimates of dispersion curves from bootstrap	12

1. SUMMARY

We performed ambient noise tomography of China using the data from the China National Seismic Network and surrounding global and PASSCAL-type stations. We used a total number of 1091 stations over the time period of 1991 to 2007. The results are summarized below. (1) Dispersion measurements. For most of the station pairs, we retrieve good Rayleigh waveforms from ambient noise correlations using a few months to several years of continuous data at all distance ranges across the entire region (over 5000 km) and for periods from about 70 s down to about 8 s. We obtained a total number of 33,800 station-pairs (paths) and measured Rayleigh wave group and phase velocities. The total number of group velocity measurements is 383,000 over 27 periods with maximum of 21,900 measurements at 20 s. (2) Dispersion maps. We inverted the Rayleigh wave dispersion measurements for dispersion maps at periods from 8 to 70 s. The dispersion maps correlate nicely with surface geology. (3) Error estimates using bootstrap analysis. A major feature of the ambient noise method is that the whole process is completely repeatable with different time segments, which make it possible to evaluate the uncertainties. We adopt a bootstrap method to quantify the errors in the Rayleigh wave group velocity dispersion measurements and the tomographic maps. Most of the pairs show similar dispersion curves between different runs and small standard deviations, indicating good data quality and convergence of the Green function. Group velocity at long period end generally has a larger error, which is consistent with the notion that the long period needs longer time to converge. The best retrieved periods are from 10 to 30 s with the optimal period of around 15 to 20 s. Pairs with large errors do not depend on the orientations of the paths or the locations of the stations. Rather, they are associated with a few stations with large average standard errors. The likely causes are missing data and poor instrumentation (or site conditions). Where ray coverage is good, there is only subtle difference in tomography maps between different runs, suggesting that our solution is very stable. (4) 3D structure. We invert the Rayleigh group and phase dispersion maps for 3D shear-wave velocity structure. The 3D model shows some remarkable features, including slow sedimentary layers of all the major basins in China at the shallow depth, Moho depth variation, fast (strong) mid-lower crust and mantle lithosphere in major basins surrounding the Tibetan Plateau (TP) (Tarim, Ordos, and Sichuan). These strong blocks thus seem to play an important role in confining the deformation of the TP to be a triangular shape. The Moho change from plateau to the marginal basins (Tarim and Sichuan) is rapid, corresponding to the rapid change of the surface topography. In northwest TP, slow anomalies extend from shallow crust to mantle lithosphere (at least 100 km). Widespread, prominent low-velocity zone is observed in mid-crust in much of the TP, but not in the margin areas, consistent with the crustal channel flow model.

2. INTRODUCTION

The overall objective of this project is to obtain surface wave dispersion measurements from ambient seismic noise correlations of the Chinese backbone stations (CNSN) and use these measurements to produce surface wave dispersion maps of China. More specifically, the objectives are: (1) to obtain dispersion measurements between CNSN

stations; (2) to obtain dispersion measurements between CNSN and FDSN, regional networks, and temporary stations; (3) to obtain dispersion maps from these dispersion measurements.

This project uses the so called “ambient noise tomography” (ANT) method, which is based on the ability to estimate surface-wave Green functions by cross-correlating long sequences of ambient seismic noise (Shapiro and Campillo 2004; Shapiro et al., 2004). The ANT method overcomes several important limitations of conventional methods based on earthquakes; i.e., uneven distribution of earthquake sources, uncertainty in earthquake location, and attenuation of short-period surface waves. Thus, the method is particularly useful for surface-wave path calibration and for tomographic mapping in aseismic regions especially at short periods (below 30 s). The expanded measurements and tomographic maps are important for improving capability for detecting and monitoring small events using the Ms: mb discriminant by improving path calibration of surface wave propagation, particularly in aseismic areas.

The projects focus on the study region of the whole China. Although our initial interest was to focus on the new Chinese backbone stations, we have added almost all the available continuous data in the IRIS DMC over the years. In Section 3 we present the ambient noise tomography method used to obtain the dispersion measurements and maps and the data sets used. Section 4 contains test results and discussion. Concluding remarks are presented in Section 5.

3. TECHNICAL APPROACH

3.1 Ambient noise tomography method

Theoretical and laboratory studies have shown that the Green functions of a structure can be obtained from the cross-correlation of diffuse wavefields (e.g., Lobkis and Weaver, 2001; see also review Campillo, 2006). The basic idea is that ballistic waves preserve, regardless of scattering, a residual coherence that can be stacked and amplified to extract coherent information between receivers. The idea has found rapid application in seismology. In particular, surface waves have been found to be easily retrievable from the cross-correlations of seismic coda (Campillo and Paul, 2003) or ambient noise (Shapiro et al., 2005; Sabra et al., 2005) between two stations. Both Rayleigh waves and Love waves can be retrieved. The new type of data has been used for tomographic mapping at regional or local scales and on continental scales. Most studies have focused on Rayleigh wave group velocity tomography from ambient noise. However, the method is applicable to Love waves and phase velocity measurements.

We use the data processing and imaging techniques described in great detail by Bensen et al. (2007). Below is a brief outline of our data procedure (Zheng et al., 2008).

First, we obtain the empirical Green function (EGF) from ambient noise cross-correlation. Continuous data are pre-processed before correlation and stacking, which

includes clock synchronization, removal of instrument response, time-domain filtering, temporal normalization and spectral whitening. The purpose is to reduce the influence of earthquake signals and instrument irregularities and to enhance the strength and bandwidth of the ambient noise correlations. We perform time domain normalization by normalizing the time series by a running average. The running average is computed between 15 and 25 sec period, a band in which small earthquakes are typically stronger than microseismic noise. Bensen et al. (2007) tested it versus sign bit normalization and found it superior in the presence of numerous small earthquakes within the seismic array. Cross-correlations are done daily and then stacked over all time periods (18 months). All the processes are linear, so breaking the cross-correlation into daily procedures, rather than performing over 1.5 year long time series, is merely a bookkeeping device. The correlation function is often asymmetric with respect to the positive and the negative delays because of non-uniform distribution of noise sources. We use the symmetric component of the correlation as the EGF by averaging the causal and acausal parts of the correlation.

Second, if the signal-to-noise ratio (SNR) is sufficiently large, Rayleigh wave group speeds are then measured using a frequency-time analysis (Ritzwoller and Levshin, 1998).

Finally, the inter-station dispersion measurements are used to invert for the Rayleigh wave group velocity maps, in exactly the same way as earthquake-based measurements.

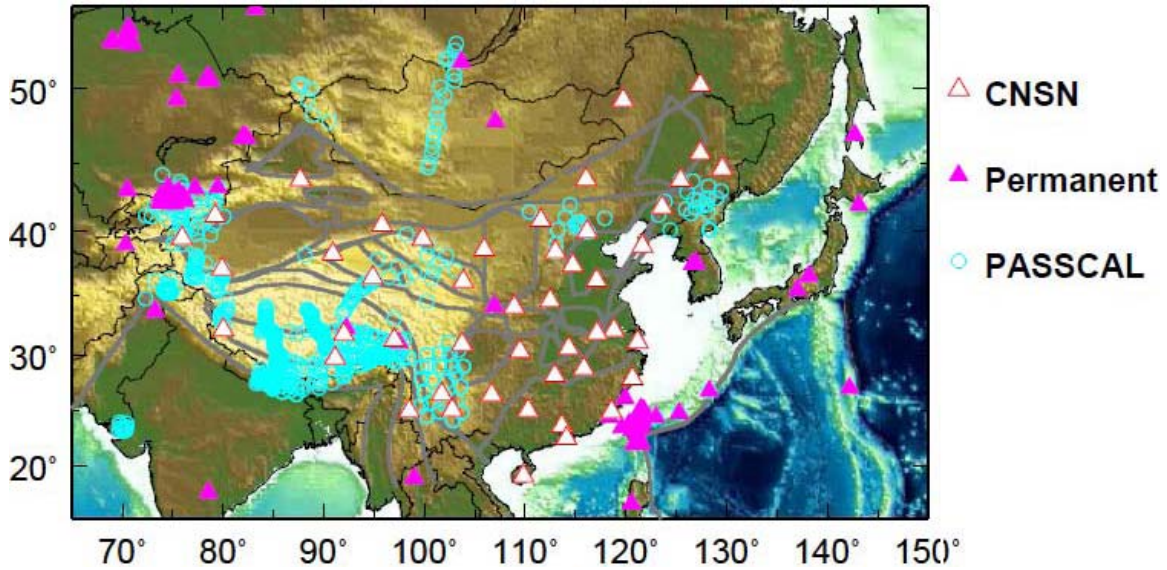


Figure 1. Distribution of seismic stations used in this study, including China National Seismic Network (CNSN) stations (solid white triangles, a total of 47), global and regional permanent stations in the surrounding regions (solid pink triangles, a total of 144), and PASSCAL-type stations (open blue triangle, a total of 880), covering the period from 1991 to 2007. Plotted in the backgrounds are topography and major tectonic boundaries and major basins from Liang et al. (2004).

3.2. Data

The data we used are shown in Figure 1. We searched for all the continuous data from 1991 to 2003, Nov 2003 through Oct 2004, and Jan-Jun 2007 in the region that are available in the IRIS data center, which included a total number of 144 permanent stations, 880 temporary PASSCAL-type stations. We used the long-period channel (LHZ) if it's available. If not, we used the BHZ channel and down sampled it to 1 sample per second.

We used 18 months of continuous data (Nov 2003 through Oct 2004 and Jan-Jun 2007) from the China National Seismic Network (CNSN) (Figure 1). The CNSN is the national backbone network with 47 stations, established around 2000, with a relatively uniform distribution across the continental China. All stations are broadband. The bandwidths of the CNSN stations are from 20 Hz to at least 120 s. We down sampled the broadband data to 1 sample per second for the construction of EGFs.

To obtain the EGF, the two stations have to overlap in time. A total of 527 stations were used in the construction of our EGFs.

4. RESULTS AND DISCUSSION

4.1 Dispersion measurements

For most of the station pairs, we are able to retrieve good Rayleigh wave signals from the ambient noise correlations (Zheng et al., 2008). Figure 2 shows typical examples of EGFs and group velocity measurements of Rayleigh waves retrieved from ambient noise correlations. Our cross-correlations show clear arrivals at different settings (near the coast or well into the continental interior) and at both relatively low frequencies (20-50 s) and high frequencies (5-20 s). The EGFs can be retrieved over the entire region (at distances of over 5000 km) (Figure 2a).

We measured group velocity dispersion curves (Figure 2c) for station pairs with Rayleigh wave $\text{SNR} > 10$. The SNR is defined as the ratio of the peak amplitude of the Rayleigh wave to the root-mean-square value of the background. The measurement is very stable. Clear dispersion can be commonly observed directly from the EGFs (Figure 2b). We found that the group velocity measurements can extend to periods of 10 s or shorter even for station pairs that are separated over thousands of kilometers. The group velocities of the HTA-BRVK path (Figure 2b,c), which samples the Tarim Basin, agree with a global 3D earthquake-based model (Shapiro and Ritzwoller, 2002) at longer periods but differ significantly at short periods (below 30 s). The slow group velocities at short periods are caused by the thick sediments of the Tarim Basin (see discussion below).

We have obtained dispersion measurements with $\text{SNR} > 10$ for periods 8 s to 72 s (Figure 3, left). The best observed frequency band is 10 to 30 s with a retrieval rate of 50 to 80%

of all the possible pairs. The ray paths provide good coverage of almost the entire Chinese continent except at the margins (Figure 3, right). The total number of measurements are 383,000 for group velocities at 27 periods, 363,800 phase velocity at 27 periods. The maximum measurements are 21,900 for both group and phase velocities at 20 s.

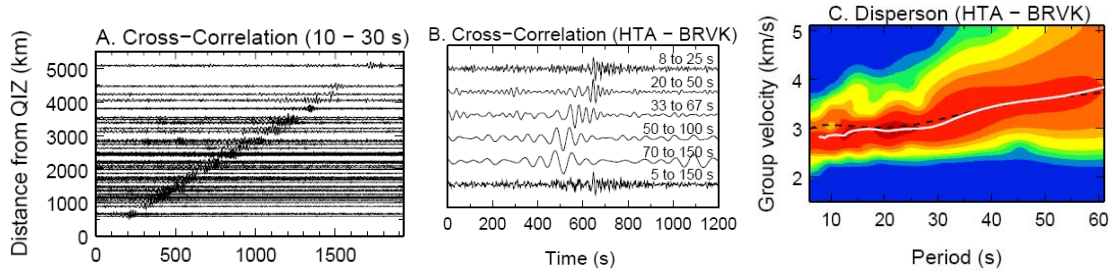


Figure 2. Example of Rayleigh wave EGFs and dispersion measurements obtained from ambient noise correlations. **(a)** Symmetric component of the correlations between station QIZ (in Hainan Province, China) and other stations. The traces are band-pass filtered at relatively short periods (10-30 s). **(b)** EGFs filtered in different frequency bands. Long-period surface waves are clearly faster than short-period ones. The path is between HTA (bordering Tarim in the south) and BRVK (Borovoye, Kazakhstan). **(c)** Frequency-time analysis (Ritzwoller and Levshin, 1998) used to retrieve Rayleigh wave group velocity dispersion curve (white) for the HTA-BRVK path. The black dashed curve is the prediction from the 3D global shear velocity model of Shapiro and Ritzwoller (2002), which is used for phase-matched filtering in the data analysis and for comparison with measurements.

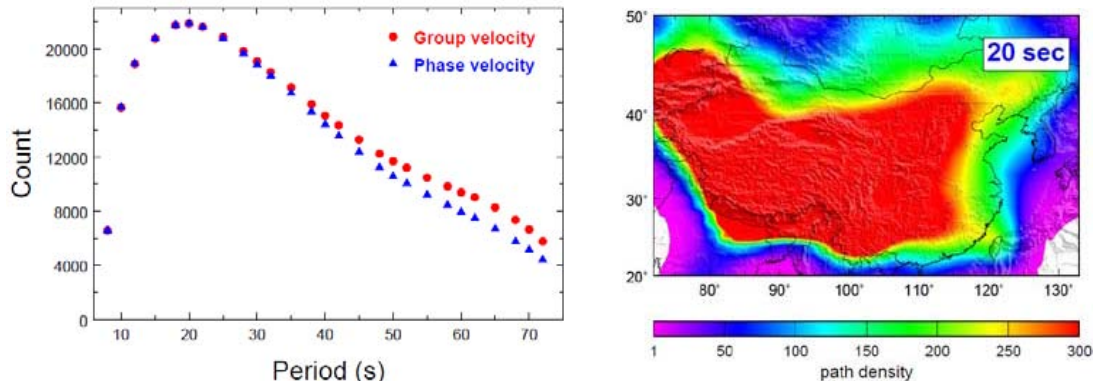


Figure 3. Distribution of Rayleigh group (solid) and phase (dashed) dispersion measurements for different periods **(left)** and ray density map for Rayleigh group dispersion measurements at the period of 20 s **(right)**. The ray density is the number of rays inside 1 degree by 1 degree cell. The rays are station pairs for which dispersion measurements have been obtained. The ray coverage is best for periods 10 to 30 s. Coverages for shorter or longer periods deteriorate.

4.2. Rayleigh wave tomography

The ray coverage of our dispersion measurements is sufficient for us to invert for Rayleigh wave group velocity maps at periods from 8 s to 60 s (Figure 4). The results show features that correlate with large-scale geological structures of China (discussed in more detail in Zheng et al., 2008). Major basins are well delineated with low velocities at short periods (8 to 20 s), including Bohai-Wan Basin (North China Basin), Sichuan Basin, Qaidam Basin, and Tarim Basin. The stable Yangtze Craton also shows up well with high velocities. At longer periods (25-50 s), the group velocity maps display striking bimodal distribution with high velocity in the east and low velocity in the west, which corresponds very well with the thinner crust in the east and much thicker crust in the west (e.g. Liang et al., 2004) as in global reference model CRUST 2.0 (<http://mafi.ucsd.edu/Gabi/rem.html>). The NNE-SSW trending boundary between fast and slow velocities (around longitude 108°E) coincides with the sharp topographic change and with the well-known Gravity Lineation.

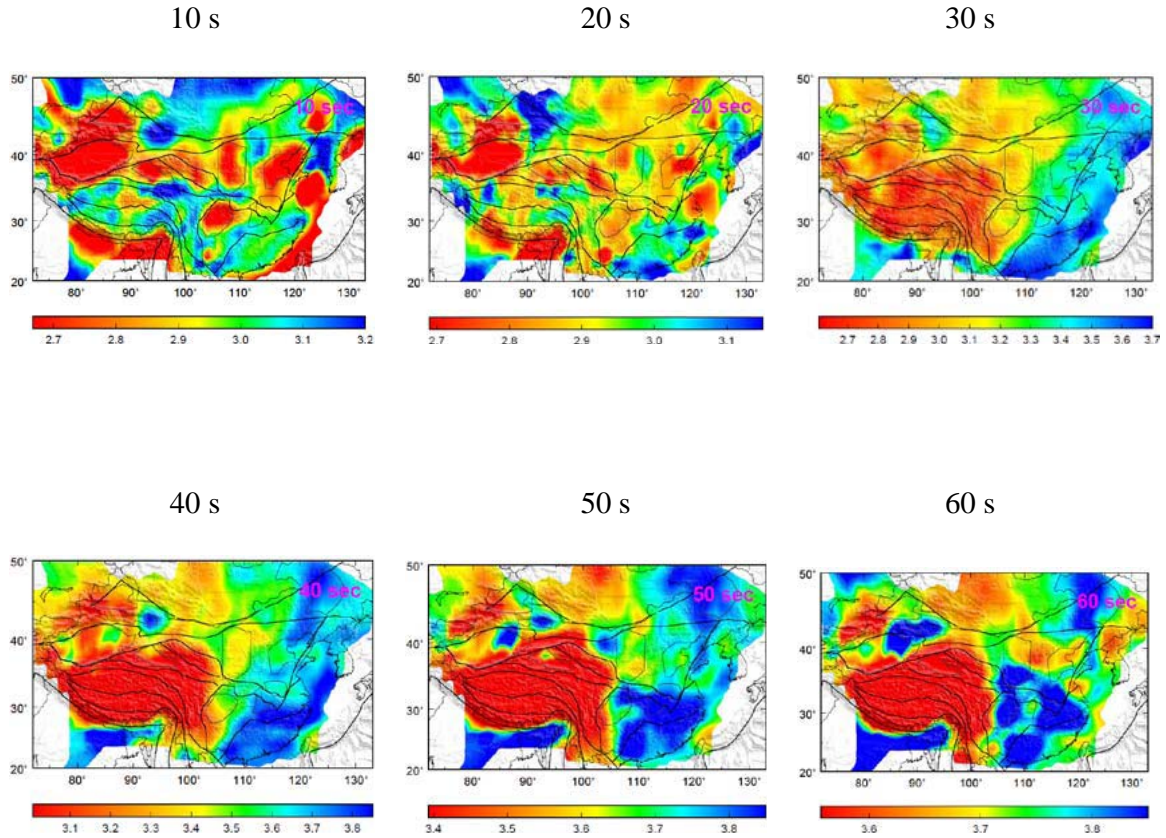


Figure 4. Rayleigh wave group velocities obtained in this study. Shown are the maps at periods 10 to 60 s, respectively. Plotted in the background are major block boundaries and basin outlines (Figure 1).

The resolutions of the Rayleigh wave group velocity maps are shown in Figure 5. The resolutions are best for 10-30 s with resolution of 200 km in most areas. The resolution decreases for longer periods, resulting from decreased number of dispersion measurements (Figure 3). However, the resolution is still better than 400 km at 60 s.

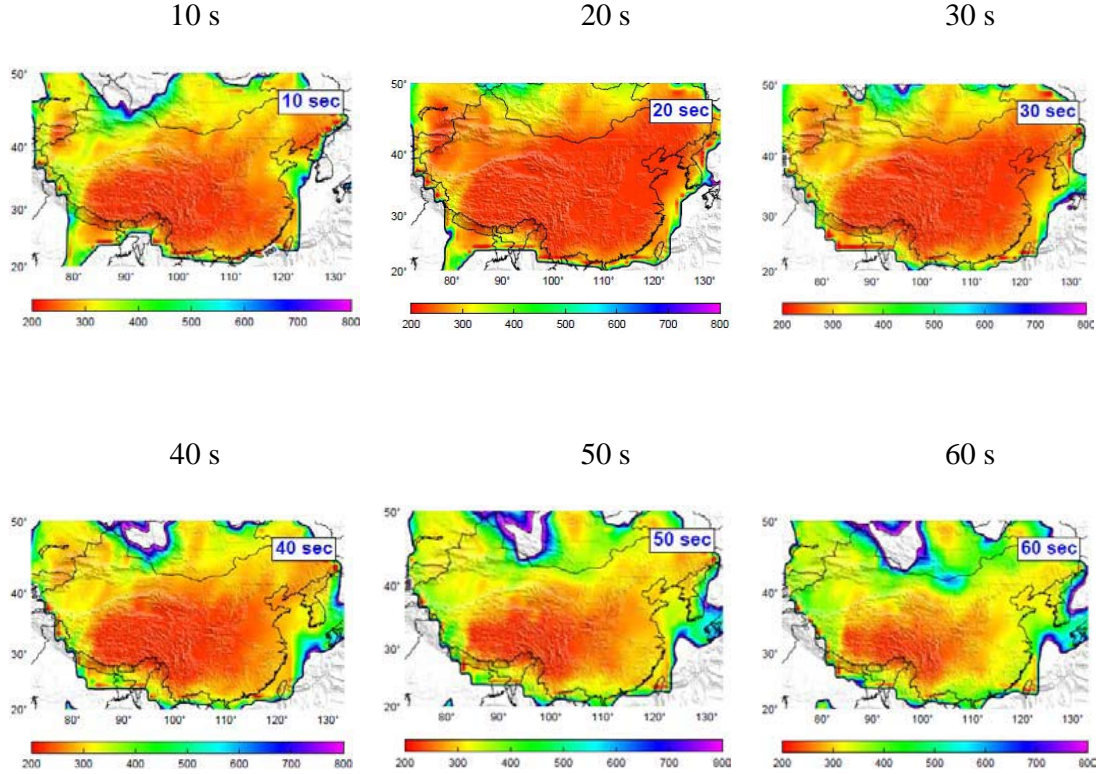


Figure 5. Resolution maps of Rayleigh wave group velocities at periods of 10 s to 60 s, respectively. The color scale is in km.

4.3. 3D shear-wave structure

We use the Rayleigh wave group and phase velocity maps (8-72 s) obtained from the ANT to invert for 3D S structure (Figure 6). The inversion is done using the programs of Herrmann of St. Louis U. The inversion results show some remarkable features for continental China and in particular the Tibetan Plateau (TP), including slow sedimentary layers of all the major basins at the shallow depth, striking east-west contrasts in Moho depth variation and lithosphere thickness, fast (strong) mid-lower crust and mantle lithosphere in major basins surrounding the TP (Tarim, Ordos, and Sichuan) (in contrast, the Qaidam Basin does not have such a “deep root”). These strong blocks thus seem to play an important role in confining the deformation of the TP to be a triangular shape. The Moho change from plateau to the marginal basins (Tarim and Sichuan) is rapid, corresponding to the rapid change of the surface topography. In the northwest TP, slow anomalies extend from shallow crust to mantle lithosphere (at least 100 km).

Extremely slow S velocities mark the mid-crust in much of the central, eastern, and southeastern TP. These slow velocities are widespread and often (but not always) connected in a laminar form. They seem to reach to the surface at certain localities in western, southern, northern, and southeastern margins. The mid/lower crust low velocity zone provides support for the channel flow model that has been proposed for the outward growth and uplift of the TP (e.g. Clark and Royden, 2000) and for the extrusion of crustal materials to the surface (e.g., Beaumont et al., 2001).

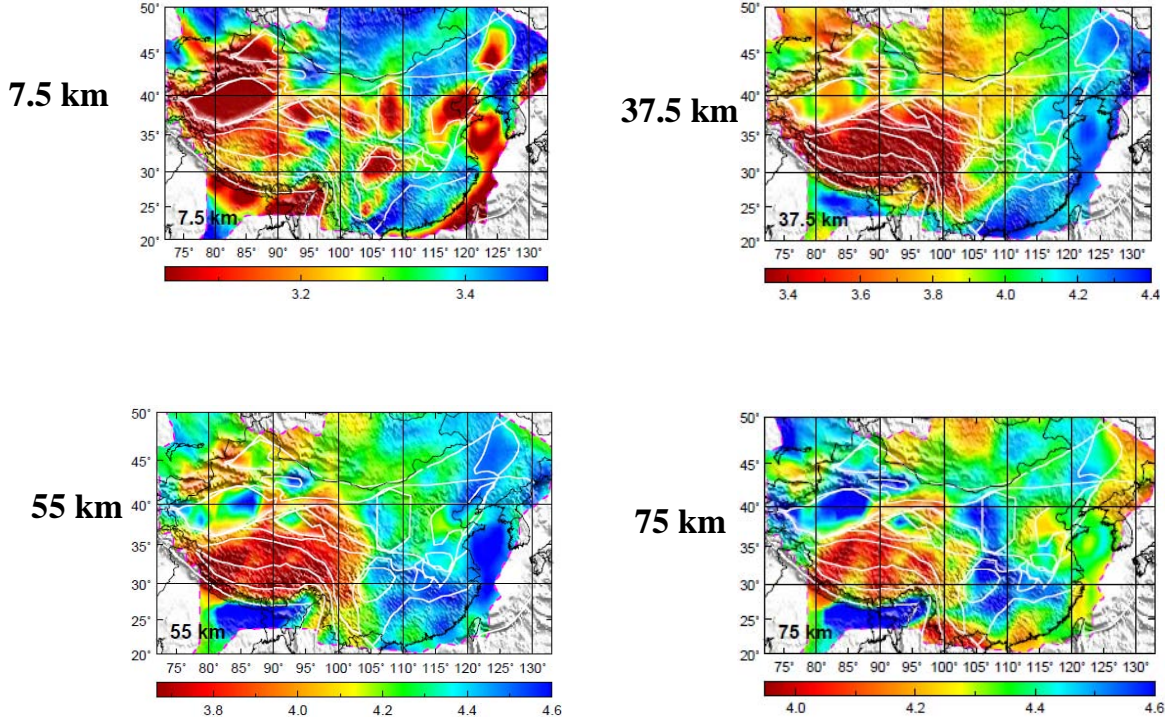


Figure 6. Inversion results of S velocity at 7.5, 37.5, 55, and 75 km. The inversion is based on Rayleigh wave group and phase dispersion maps. Dispersions for each grid (1x1 degree) are extracted from the Rayleigh wave group and phase maps.

The S velocity model we have derived can be used to explore the model characters and tectonic implications. Because of the apparent correlation of the S velocities and crustal thickness, one useful exercise is to derive a crustal thickness model based on the Vs model. If we obtain the Vs that corresponds to the depth of the Moho as defined by the reference model CRUST 2.0, we find that the average of the S velocities is nearly constant (Figure 7). We thus use the linear trend as a calibration of using the S velocity to find the true Moho (The linear trend has nearly the same Vs value with only a small positive slope). Thus to find the true Moho for any given point, we follow the steps: (1) Find the reference Moho depth from CRUST 2.0, (2) find the reference Vs from the linear trend, and (3) find the depth that corresponds to the reference Vs (and close to the

CRUST 2.0 depth). The procedure ensures that the newly derived Moho map (Figure 8, left) is similar to the CRUST 2.0 (Figure 8, right) overall, but the new map shows more detailed variations that correspond to variation in S velocities.

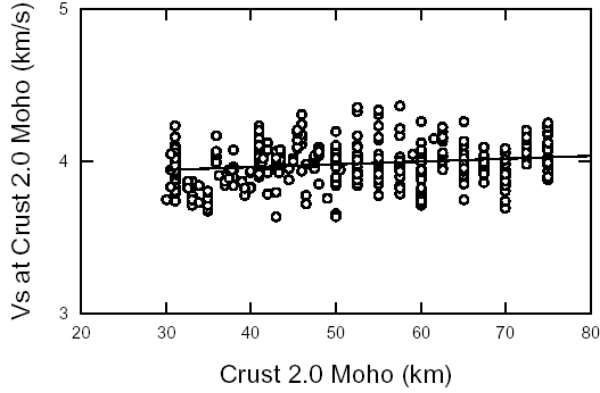


Figure 7. S velocities at the depth of CRUST 2.0 Moho that are retrieved from our S model.

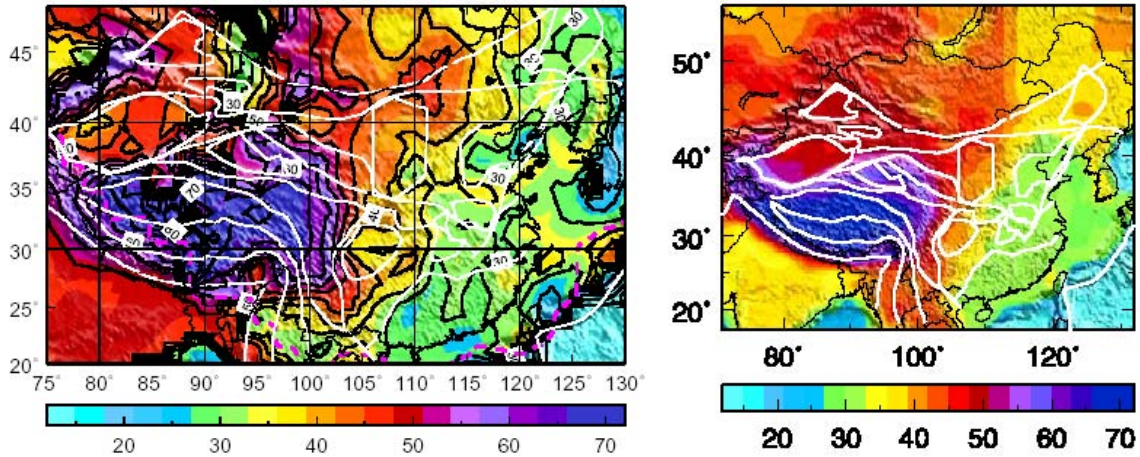


Figure 8. Crustal thickness map derived from the S velocity model (left), in comparison to reference CRUST 2.0 model (right). Note the map scales are different.

4.4. Validation and error analyses

Comparison of the tomographic maps with the geological features discussed above provides an important initial validation of the ANT methodology; i.e., the method provides models of group wave speeds that are consistent with well-known geological features and other geophysical observations. Furthermore, the complete repeatability of the ANT method makes it possible to directly validate the methodology and to evaluate the uncertainties of the dispersion measurements. We have examined the errors of our

dispersion measurements and tomography in a variety of ways (see a summary by Zheng et al., 2008). The methods include the following. (1) Validation with surface observables. Comparison of the tomographic maps with the geological features discussed above provides an important initial validation of the ambient noise tomography (ANT) methodology; i.e., the method provides models of group wave speeds that are consistent with well-known geological features and other geophysical observations. (2) Direct validation with surface wave generated by an earthquake along the same path (e.g., Shapiro et al., 2005; Bensen et al., 2007). (3) Comparing EGFs obtained from ambient noise and that from seismic coda (Yao et al., 2006). (4) Temporal stability: Comparing the EGFs from the data observed at different time periods (e.g., different months) (Shapiro et al., 2005; Yao et al., 2006; Bensen et al., 2007). Furthermore, because the principal ambient noise sources are believed to come from the oceans, and are seasonal, the consistency of the correlations from different seasons gives a measure of the stability and error of the EGFs. (5) Spatial consistency: Comparing station-pairs along similar paths (Bensen et al., 2007). The EGFs between a far-away station to two or more stations that are close to one another should be similar as the paths sample similar structure. We have examined temporal and spatial consistency of our dispersion measurements and found that they are very consistent whenever the SNRs of the EGFs are high (see examples in Zheng et al., 2008). (6) Model-based validation: comparing predictions with earthquake-based measurements. (7) Bootstrap analyses (Xu et al., 2008) (see below).

Examination of temporal and spatial consistency of our dispersion measurements suggest that they are very consistent whenever the SNRs of the EGFs are high. Some examples are shown in Figure 9. The temporal comparisons include a station pair with an east-west path (BJT-BRVK) and another pair with a north-south path (XAN-CHTO) (Figure 9, top). We construct 23 dispersion curves using 12 months of data with different sliding windows or using 12 months of data over different seasons. For either pair, we find the standard deviation of these curves to be less than 2% for all periods and the standard deviation of the mean to be less than 0.5%. The spatial comparisons include two pathways (Figure 9, bottom), from GOM to GZH/SZN and from WMQ to SSE/NJ2. The group velocities between WMQ and SSE are quite similar to those between WMQ and NJ2 at all the observed periods (10 to 60 s). The group velocities between GOM-GZH and GOM-SZN are also similar at periods less than 40 s. At periods greater than 40 s, they are somewhat different but are within their temporal uncertainties.

An example of model-based validation is shown in Figure 10. We see generally good agreements between the predicted dispersion curves based on the dispersion maps and the observations for this path.

Bootstrap analyses. The retrieval of the surface wave EGF relies on the stacking of cross correlation of continuous data for long enough time series. The total length of data required for the Green function to converge is empirical and highly frequency dependent: generally the longer the period the longer the time is needed. Furthermore, the ambient noise source and station site conditions (including instrumentation stability) are uncertain. We have recently proposed a bootstrap method to quantify the errors in Rayleigh group velocity dispersion measurements and group velocity tomographic maps,

based on the complete repeatability of the ambient noise correlation and tomography process (Xu et al., 2008).

Our bootstrap analysis follows the following steps. 1) We obtain the EGF using one month of data for each of the 18 months. 2) We select 18 random months among the months that we have data. The selection process is a random sampling with replacement as in any bootstrap methods. We then obtain the stacked EGF using the EGFs of these months for each and every station pair. Using these stacked GFs, we measure dispersion curves for all station pairs and construct tomographic maps as usual. 3) We repeat the step 2 for 50 times. 4) We obtain the mean and the standard deviation of the dispersion curve for each station pair from the 50 dispersion curves obtained in step 3. We regard the mean and the standard deviation as the group velocity estimate and the associated error. 5) Similarly, we obtain the standard errors of our tomographic models using the models obtained from the 50 iterations described in steps 2 and 3.

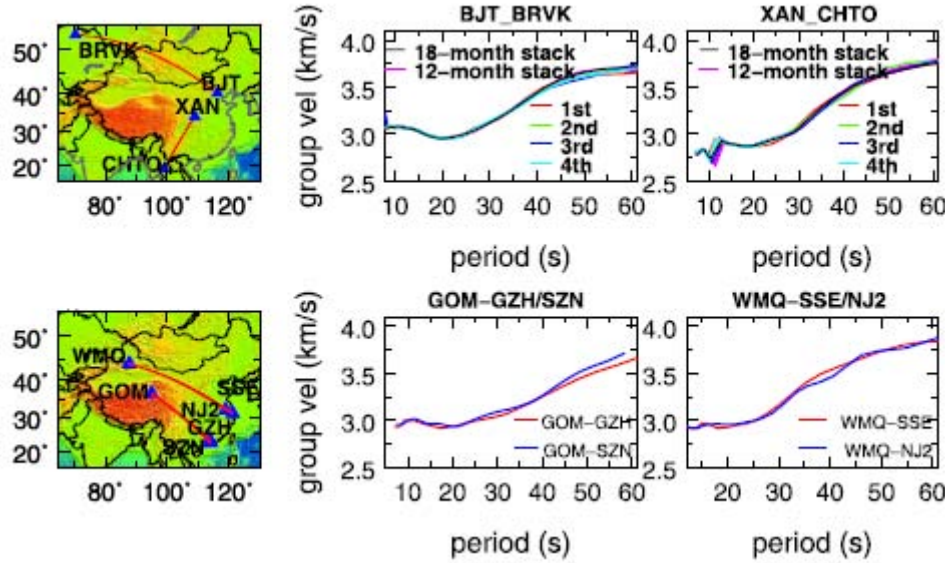


Figure 9. Temporal (top) and spatial (bottom) consistency of dispersion measurements. (Top) Dispersion curves from different time windows. We select two pairs, BJT-BRVK along an east-west path and XAN-CHTO along a north-south path. For either pair, we calculate two sets of EGFs. For each calculation of the EGF, a total of 12 months of data are used. The 18-month stack (including all the data we collected) is plotted for comparison. One set uses seasonal data (red, green, blue, and cyan), i.e., data from the same season over a period of 4 years. The other set uses 12 months of data with a sliding time window of 10 days (total of 19 curves, all in magenta). (Bottom) Dispersion curves between a far-way station and two close stations. We select two pathways, one from GOM to GZH/SZN (distance about 2400 km) and the other from WMQ to SSE/NJ2 (distance about 3100 km). The distance between GZH and SZN is about 133 km, and that between SSE and NJ2 is 245 km.

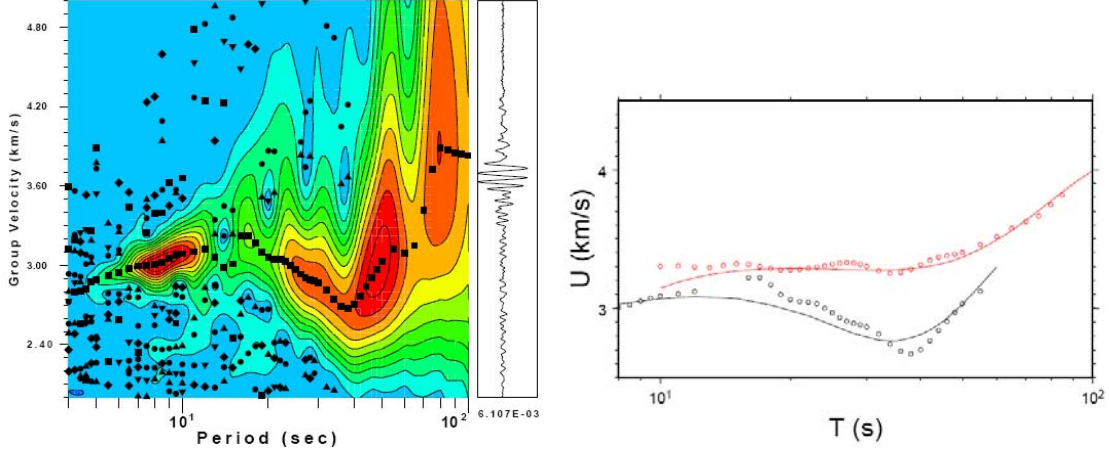


Figure 10. Example of model validation. (Left) Retrieval of Rayleigh wave group velocity of a 2008 Wenchuan aftershock at Lhasa station. (Right) Comparison of observed (dots) and predicted group velocities of Rayleigh (black) and Love (red) waves along the path. Lines are predictions for the ambient noise tomographic model.

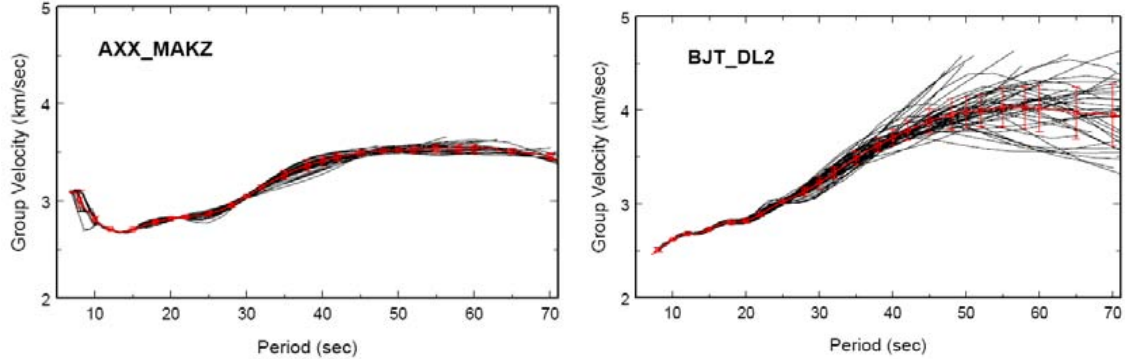


Figure 11. Examples of error estimates of dispersion curves from bootstrap with a good pair (left) and a bad pair (right). Black curves are dispersion measurements for all the 50 runs. Red curves are the mean values. Error bars at different periods indicate the standard deviations. For the good pair (AXX-MAKZ), dispersion curves for different runs are very close to each other. The standard deviations are small throughout the whole periods. For the bad pair (BJT-DL2), dispersion curves spread out at long periods. The large standard deviations at long periods indicate large errors in the measurements.

Figure 11 shows two examples of error estimates of the dispersion curves using the bootstrap method. Most pairs show similar dispersion curves between different runs and small standard deviation (generally less than 0.1 km/s), indicating good data quality and convergence of the Green function. Group velocity at a long period generally has a larger error, which is consistent with the notion that the long period needs longer time to converge.

There is only subtle difference in tomography maps between different runs, suggesting that our solution is very stable. Standard deviation in the region with good ray coverage is small (generally less than 0.1 km/s), indicating a stable and reliable solution in well-sampled regions. The Rayleigh waves are best retrieved from 10 to 30 s with the best

periods around 15 to 20 s. A pitfall of the model error estimates is that the standard deviations in the regions with poor ray coverage (at the margins) are also small, due to regularization in the tomographic inversion process. Our tomographic inversion includes regularization using a prior model. Thus the inversions for the poorly sampled regions from different runs all converge to the prior model, giving an artifact of small errors.

We found that the pairs with large variations do not have a preferred orientation or a particular geographical location. Rather, these pairs are generally associated with a few stations with large standard deviations. We derive average standard deviation of the surface wave velocity for each station at each period by averaging over all the pairs associated with that station. The exercises provide a way to identify and sort out good and poor stations efficiently.

5. CONCLUSIONS

The primary objective of this contract was directed toward new inter-station dispersion measurements and tomography based on measurements using the ANT method. We expanded greatly beyond the original goals. We expanded CNSN data from the original 1 year to 18 months and expanded the data search time period from the original 3 years to almost the entire period (1991-2007) of new data availability in the IRIS data center. We more than doubled the expected number of stations (443) to over a thousand. The results are a vast collection of new dispersion measurements and much refined tomographic maps. We tested out new bootstrap methods to characterize errors of dispersion measurements and tomography, which suggested robust results, giving us confidence in the measurements and tomography. The S wave 3D model from the dispersion maps shows many significant features of the geology of the region. Continuing understanding of these features will not only be important for science but for monitoring and discrimination as well.

REFERENCES

- Beaumont, C., R.A. Jamieson, M.H. Nguyen, et al., Himalayan tectonics explained by extrusion of a low-viscosity crustal channel coupled to focused surface denudation, *Nature*, 414, 738-742, 2001.
- Benson, G., M. Ritzwoller, M. Barmin et al. (2007), Processing seismic ambient noise data to obtain reliable broad-band surface wave dispersion measurements, *Geophys. J. Int.*, 169(3), 1239-1260.
- Campillo, M. Phase and correlation in random seismic fields and the reconstruction of the Green function, *Pure Appl. Geophys.*, 163, 475-502, 2006.
- Campillo M. and A. Paul, Long-range correlations in the diffuse seismic coda, *Science*, 299, 547-549, 2003.
- Clark, M.K., and L.H. Royden, Topographic ooze: Building the eastern margin of Tibet by lower crustal flow, *Gelogy*, 28, 703-706, 2000.
- Laske, G., and G. Masters, A global digital map of sediment thickness, *EOS Trans. AGU*, 78, F483, 1997.
- Liang C., X.D. Song, and J.L. Huang, Tomographic Inversion of Pn Travel-Times in China, *J. Geophys. Res.*, 109, B11304, doi. 10.1029/2003JB002789, 2004.
- Lobkis, O.I., and R.L. Weaver, On the emergence of the Greens function in the correlations of a diffuse field, *J. Acoust. Soc. Am.*, 110, 3011-3017, 2001.
- Ritzwoller, M.H. and A.L. Levshin, Eurasian surface wave tomography: Group velocities, *J. Geophys. Res.*, 103, 4839-4878, 1998.
- Sabra, K.G., P. Gerstoft, P. Roux, W.A. Kuperman, and M.C. Fehler, Surface wave tomography from microseisms in Southern California, *Geophys. Res. Lett.*, 2005.
- Shapiro, N.M. M. Campillo, L. Stehly, and M.H. Ritzwoller, High resolution surface wave tomography from ambient seismic noise, *Science*, 307(5715), 1615-1618, 2005.
- Shapiro, N.M. and M.H. Ritzwoller, Monte-Carlo inversion for a global shear velocity model of the crust and upper mantle, *Geophys. J. Int.*, 151, 88-105, 2002.
- Song, X.D., X.L. Sun, S.H. Zheng, Z. J. Xu, M. Ritzwoller, Y.J. Yang, Surface Wave Dispersion Measurements and Tomography from Ambient Seismic Noise in China, *Monitoring Research Reviews*, Portsmouth, Virginia, 2008.
- Xu, Z., X.D. Song, S.H. Zheng, M.H. Ritzwoller, Bootstrap analysis on surface wave dispersion and tomography derived from ambient noise cross-correlation, *IRIS Workshop*, Skamania Lodge, Stevenson, WA, 2008.
- Yao, H. J., R. D. van der Hilst, and M. V. de Hoop, Surface-wave array tomography in SE Tibet from ambient noise and two-station analysis - I. Phase velocity maps, *Geophys. J. Int.*, 166(2), 732 – 744, doi:10.1111/j.1365-246X.2006.03028.x, 2006.
- Zheng, S.H., X.L. Sun, X.D. Song, Y.J. Yang, M.H. Ritzwoller, Surface wave tomography of China from ambient seismic noise correlation, *Geochem. Geophys. Geosyst.*, 9, Q05020, doi:10.1029/2008GC001981, 2008.

List of Symbols, Abbreviations, and Acronyms

AFRL	Air Force Research Laboratory
AFSPC	Air Force Space Command
AFWA	Air Force Weather Agency
CNSN	China National Seismic Network
DMC	Data Management Center
EGF	Empirical Green Function
FDSN	International Federation of Digital Seismograph Networks
IRIS	International Research Institution of Seismology
PASSCAL	Program for Array Seismic Studies of the Continental Lithosphere
SNR	Signal-to-Noise